Electron-impact single ionization of the Se^{3+} ion

S. Pakalka, S. Kučas, Š. Masys, A. Kynienė, A. Momkauskaitė, and V. Jonauskas*
Institute of Theoretical Physics and Astronomy, Vilnius University, Saulėtekio av 3, LT-10257 Vilnius, Lithuania

(Received 29 October 2017; published 31 January 2018)

Single ionization by electron impact of the Se^{3+} ion is investigated in the Dirac-Fock-Slater approximation. Contributions from direct ionization (DI), excitation-autoionization, and resonant-excitation double-autoionization processes are taken into account. Good agreement with the experiment is obtained at the lower energies of the incident electron when the DI process is considered in the potential of the ionizing ion. On the other hand, the potential of the ionized ion has to be used for the higher energies of the electron. It is shown that ionization-ionization and ionization-excitation-ionization processes can play the significant role in the double ionization of Se^{3+} ions.

DOI: 10.1103/PhysRevA.97.012708

I. INTRODUCTION

Spectral lines from selenium ions observed in planetary nebulae [1–3] raise demand of reliable atomic data needed for modeling the spectra. In addition to photoionization, autoionization, and dielectronic recombination, electron-impact ionization is one of the processes having an effect upon the gas ionization degree in the nebulae. Single ionization by electron impact is a stronger process compared to the double ionization; besides, study of the latter is quite complicated due to the complex nature of the four-body Coulomb problem [4–7].

Recently, experimental cross sections by electron impact for the Se^{2+} and Se^{3+} ions have been observed for the first time using dynamic-crossed-beams technique [8,9]. Previous experimental studies of ionization process for selenium ions have been focused on interaction with photons [10–13].

First theoretical results for electron-impact single- and double-ionization cross sections for the Se^{2+} and Se^{3+} ions have been produced using a configuration-average distorted-wave (CADW) method [14]. Essential discrepancies among theoretical and experimental cross sections for single ionization of Se^{3+} have been obtained for lower and higher energies of the incident electron. Later, single-ionization cross sections have been calculated using the level-to-level distorted-wave (LLDW) method for the ground and excited configurations [15] having an aim to explain the obtained discrepancies in the CADW calculations. They suggested that contribution of 15% from the excited $[Ar]3d^{10}4s^24d$ configuration is seen in the experimental data. Unfortunately, as we show below, none of the $[Ar]3d^{10}4s4p^2$ or $[Ar]3d^{10}4s^24d$ configurations have long-lived energy levels.

The main aim of the current work is to study electron-impact single ionization of the Se^{3+} ion by considering the direct ionization (DI), excitation-autoionization (EA), and resonant-excitation double-autoionization (REDA) processes within the LLDW framework. What is more, investigation of the ionization cross sections for the W^{17+}, W^{27+}, and W^{26+} ions [16–18] has demonstrated that the DI Maxwellian rate coefficients are slightly larger for the semirelativistic values compared to the data from the Dirac-Fock-Slater (DFS) calculations. However, the EA rate coefficients were smaller for the semirelativistic approximation. Previous studies dealt with heavy elements where relativistic effects are of large importance. Therefore, it is important to estimate these effects for other ions.

The rest of the paper is organized as follows. In the next section, we describe theoretical methods used for the atomic structure and scattering calculations that are performed to determine total single-ionization cross sections for the Se^{3+} ion. In Sec. III, the obtained results are discussed.

II. THEORETICAL APPROACH

Energy levels, radiative and Auger transition probabilities, electron-impact excitation, and ionization cross sections are determined using the flexible atomic code (FAC) [19], which implements the DFS approximation. Bound wave functions are obtained separately for each charge state using the self-consistent field procedures. The DW approach is applied for the investigation of the electron-impact excitation and ionization processes. It has to be noted that the Auger transition probabilities and electron-impact ionization cross sections are obtained using the wave functions from the different charge states. The nonorthogonality of the wave functions from different ionization stages is expected to have only a minor influence on the data. It was demonstrated that additional terms introduced in the relevant matrix element are small, often have different signs, and approximately cancel out when summed [20].

Direct and indirect processes are investigated to obtain total electron-impact single-ionization cross sections. Two indirect processes are considered in this work: EA and REDA. In the direct process, the electron is removed from the atomic system instantly. On the other hand, the EA process occurs when the atomic system is excited to the autoionizing state which decays to the next ionization stage through Auger transitions. Thus total electron-impact single-ionization cross section from the level i of A^{q+} ion to the level j of $A^{(q+1)+}$ ion can be expressed

*valdas.jonauskas@tfai.vu.lt

by the following equation:

$$\sigma_{ij}(\varepsilon) = \sigma_{ij}^{\mathrm{DI}}(\varepsilon) + \sigma_{ij}^{\mathrm{EA}}(\varepsilon) + \sigma_{ij}^{\mathrm{REDA}}(\varepsilon)$$

$$= \sigma_{ij}^{\mathrm{DI}}(\varepsilon) + \sum_k \sigma_{ik}^{\mathrm{CE}}(\varepsilon) B_{kj} + \sum_{kl} \sigma_{il}^{\mathrm{DC}}(\varepsilon) B_{lk} B_{kj}, \quad (1)$$

where $\sigma_{ij}^{\mathrm{DI}}(\varepsilon)$ is the DI cross section at the incident electron energy ε, $\sigma_{ij}^{\mathrm{EA}}(\varepsilon)$ is the cross section for the EA process, $\sigma_{ik}^{\mathrm{CE}}$ is the collisional excitation (CE) cross section to the level k of the A^{q+} ion, and $\sigma_{ij}^{\mathrm{DC}}(\varepsilon)$ is the cross section for the dielectronic capture (DC) to the level l of the $A^{(q-1)+}$ ion [21]. The summation over all final levels j in Eq. (1) leads to the total ionization cross section for the initial level i.

Our study of DI channels includes ionization from the $3d$, $4s$, and $4p$ shells of the ground configuration:

$$[\mathrm{Ar}]3d^{10}4s^2 4p + e^- \rightarrow [\mathrm{Ar}] \begin{Bmatrix} 3d^9 4s^2 4p \\ 3d^{10} 4s\ 4p \\ 3d^{10} 4s^2 \end{Bmatrix} + 2e^-. \quad (2)$$

The DI cross sections are studied in the potential of the ionizing (V^N, where N is the number of electrons in the initial target configuration) and ionized (V^{N-1}) ions [19].

EA presents the two-step process: excitation with subsequent autoionization. Autoionization branching ratio B_{kj} is included in the calculations to take into account all possible radiative and Auger transitions from the excited state:

$$B_{kj} = \frac{A_{kj}^{\mathrm{a}} + \sum_n A_{kn}^{\mathrm{r}} B_{nj}}{\sum_m A_{km}^{\mathrm{a}} + \sum_n A_{kn}^{\mathrm{r}}}, \quad (3)$$

where A^a and A^r are the Auger and radiative transition probabilities, respectively. It is clear that excitations to the levels which cannot decay through the Auger transitions directly or through the intermediate states do not contribute to the EA process. The radiative transitions from the excited state diminish cross sections of the indirect process. Thus study of radiative decay in the EA process is called the radiative damping.

The term $\sum_n A_{kn}^{\mathrm{r}} B_{nj}$ in the numerator of Eq. (3) determines additional steps in the indirect ionization process: the excitation from the level i of the initial ion to level k, radiative decay from level k to level n which resides above the ionization threshold, and subsequent autoionization from level n to level j. Unfortunately, the amount of calculations drastically increases when more than two steps are considered in the investigation of the EA process. Thus the second term in the numerator of Eq. (3) is omitted in the current work.

The EA process includes excitations from the $3d$ and $4s$ shells to configurations above the single-ionization threshold. It is schematically shown as

$$[\mathrm{Ar}]3d^{10}4s^2 4p + e^- \rightarrow [\mathrm{Ar}] \begin{Bmatrix} 3d^9 4s^2 4p\ n_1 l_1 \\ 3d^{10} 4s\ 4p\ 4f \\ 3d^{10} 4s\ 4p\ 5[d,f,g,h] \\ 3d^{10} 4s\ 4p\ n_2 l_2 \end{Bmatrix} + e^-, \quad (4)$$

where $n_1 = 4-25$, $n_2 = 6-25$, $l_1 < n_1$, and $l_1, l_2 < 6$. All possible electric dipole and Auger transitions from the considered excited configurations are investigated.

The REDA process is studied to consider DC of the incident electron to the atomic system. The produced autoionizing states decay through radiative and Auger cascade in turn producing ions in various ionization stages. Contribution of DC with the subsequent Auger cascade to the next ionization stage compared to the initial one results in a single-ionization process. The REDA channels included for the $3d$ shell are as follows. The first step proceeds via the DC process:

$$3d^{10}4s^2 4p + e^- \rightarrow 3d^9 4s^2 4p\ n_1 l_1 n_2 l_2, \quad (5)$$

where $n_1 = 4$–6, $n_2 = n_1$–50, $l_1 < n_1$, $l_2 < n_2$, and l_1, $l_2 < 5$. Capture to the higher shells is not considered in the current work as our calculations show that it would not lead to considerable contribution to the REDA cross sections. We presume that the omitted excitations would not have more than 5% change in the data. As well, the DC processes which include the $3s$ and $3p$ shells are not investigated here as their contribution is much smaller compared to the excitation from the $3d$ shell.

The formed autoionizing states can decay through Auger transitions by emitting one electron to form Se^{3+}:

$$3d^9 4s^2 4p\ n_1 l_1 n_2 l_2 \rightarrow \begin{Bmatrix} 3d^{10} 4s^2\ 4p \\ 3d^{10} 4s^2\ n_3 l_3 \\ 3d^{10} 4s\ n_1 l_1 n_2 l_2 \\ 3d^{10} 4p\ n_1 l_1 n_2 l_2 \\ 3d^{10} 4s\ 4p\ n_3 l_3 \\ 3d^9 4s^2\ 4p\ n_4 l_4 \end{Bmatrix} + e^-, \quad (6)$$

where $n_3 l_3 = n_1 l_1$ or $n_3 l_3 = n_2 l_2$, $n_4 = 4$–6 and $l_4 < 5$ represents all possible distributions of the electrons in the shells formed by Auger transitions from the initial configuration. The autoionizing states from the first step of the Auger decay can then subsequently emit another electron and form Se^{4+}:

$$\begin{Bmatrix} 3d^{10} 4s\ n_1 l_1 n_2 l_2 \\ 3d^{10} 4p\ n_1 l_1 n_2 l_2 \\ 3d^{10} 4s\ 4p\ n_3 l_3 \\ 3d^9 4s^2\ 4p\ n_4 l_4 \end{Bmatrix} \rightarrow \begin{Bmatrix} 3d^{10} 4s^2 \\ 3d^{10} 4s\ n_4 l_4 \\ 3d^{10} 4p\ n_4 l_4 \end{Bmatrix} + e^-. \quad (7)$$

In a similar way, REDA which involves excitation from the $4s$ shell has been investigated to determine contribution to single-ionization cross sections.

III. RESULTS

The obtained theoretical single-ionization threshold of Se^{3+} is 42.35 eV. Energy of 108.21 eV is needed to remove two outer electrons from the ground $[\mathrm{Ar}]3d^{10}4s^2 4p^1$ configuration and reach ground configuration of the Se^{5+} ion. The single-ionization threshold is in good agreement with a value of 42.2 ± 1.8 eV determined from the experiment [8] and the NIST reference value of 42.95 eV [22]. The ground configuration of the Se^{3+} ion has only two levels. Energy of the fine splitting is 0.5668 eV (Table I) while NIST provides a slightly lower value of 0.5426 eV. The difference of about 4% between these two values can be attributed to correlation effects which are not considered in this work.

Contributions from long-lived levels are often seen in experiments for ionization cross sections [23,24]. The first two excited configurations $4s4p^2$ and $4s^24d$ of the Se^{2+} ion do not contain long-lived levels (Table I). The first long-lived

TABLE I. Energy levels and lifetimes of the five lowest configurations for Se^{3+}. The lifetimes include contribution from electric dipole, quadrupole, and octupole, as well as magnetic dipole and quadrupole transitions. Closed subshells are omitted in the notation of levels.

Index	Configuration	Level	J	Energy (eV)	τ (s)
0	$4s^24p^o$	$4p_{1/2}$	1/2	0.000	
1	$4s^24p^o$	$4p_{3/2}$	3/2	0.567	1.16×10^{0}
2	$4s4p^2$	$4s$	1/2	8.316	5.06×10^{-7}
3	$4s4p^2$	$4s\ 4p_{1/2}[0]4p_{3/2}$	3/2	8.531	1.86×10^{-6}
4	$4s4p^2$	$4s\ 4p^2_{3/2}(2)$	5/2	8.852	4.77×10^{-7}
5	$4s4p^2$	$4s\ 4p_{1/2}[0]4p_{3/2}$	3/2	13.273	4.00×10^{-10}
6	$4s4p^2$	$4s\ 4p_{1/2}[1]4p_{3/2}$	5/2	13.344	4.48×10^{-10}
7	$4s4p^2$	$4s\ 4p^2_{3/2}(0)$	1/2	15.710	2.39×10^{-10}
8	$4s4p^2$	$4s\ 4p_{1/2}[1]4p_{3/2}$	1/2	17.558	6.08×10^{-11}
9	$4s4p^2$	$4s\ 4p^2_{3/2}(2)$	3/2	17.893	5.89×10^{-11}
10	$4s^24d$	$4d_{3/2}$	3/2	18.374	9.95×10^{-11}
11	$4s^24d$	$4d_{5/2}$	5/2	18.417	1.04×10^{-10}
12	$4p^{3o}$	$4p_{1/2}4p^2_{3/2}(2)$	3/2	24.917	7.23×10^{-11}
13	$4s4p4d^o$	$4s\ 4p_{1/2}[0]4d_{3/2}$	3/2	26.069	1.66×10^{-8}
14	$4s4p4d^o$	$4s\ 4p_{1/2}[1]4d_{3/2}$	5/2	26.209	9.85×10^{-9}
15	$4s4p4d^o$	$4s\ 4p_{1/2}[1]4d_{5/2}$	7/2	26.396	9.02×10^{-9}
16	$4s4p4d^o$	$4s\ 4p_{3/2}[2]4d_{5/2}$	9/2	26.618	8.95×10^{-1}
17	$4p^{3o}$	$4p_{1/2}4p^2_{3/2}(2)$	3/2	27.273	1.71×10^{-10}
18	$4p^{3o}$	$4p_{1/2}4p^2_{3/2}(2)$	5/2	27.368	1.68×10^{-10}
19	$4s4p4d^o$	$4s\ 4p_{1/2}[0]4d_{5/2}$	5/2	27.733	1.66×10^{-10}
20	$4s4p4d^o$	$4s\ 4p_{1/2}[1]4d_{5/2}$	3/2	27.779	2.97×10^{-10}
21	$4s4p4d^o$	$4s\ 4p_{3/2}[2]4d_{5/2}$	3/2	28.014	7.34×10^{-11}
22	$4s4p4d^o$	$4s\ 4p_{3/2}[2]4d_{5/2}$	5/2	28.048	1.12×10^{-10}
23	$4s4p4d^o$	$4s\ 4p_{1/2}[1]4d_{3/2}$	1/2	28.074	5.86×10^{-11}
24	$4s4p4d^o$	$4s\ 4p_{3/2}[2]4d_{3/2}$	1/2	28.338	7.87×10^{-11}
25	$4s4p4d^o$	$4s\ 4p_{3/2}[2]4d_{5/2}$	7/2	28.380	5.34×10^{-11}
26	$4s4p4d^o$	$4s\ 4p_{3/2}[2]4d_{3/2}$	3/2	28.382	6.61×10^{-11}
27	$4s4p4d^o$	$4s\ 4p_{3/2}[2]4d_{3/2}$	5/2	28.403	5.95×10^{-11}
28	$4p^{3o}$	$4p_{1/2}4p^2_{3/2}(0)$	1/2	28.972	1.35×10^{-10}
29	$4p^{3o}$	$4p^3_{3/2}$	3/2	29.126	1.33×10^{-10}
30	$4s4p4d^o$	$4s\ 4p_{1/2}[1]4d_{5/2}$	5/2	30.142	1.49×10^{-10}
31	$4s4p4d^o$	$4s\ 4p_{3/2}[2]4d_{3/2}$	7/2	30.578	1.36×10^{-10}
32	$4s4p4d^o$	$4s\ 4p_{3/2}[2]4d_{5/2}$	3/2	30.939	1.71×10^{-10}
33	$4s4p4d^o$	$4s\ 4p_{3/2}[2]4d_{5/2}$	1/2	31.188	1.70×10^{-10}
34	$4s4p4d^o$	$4s\ 4p_{3/2}[1]4d_{5/2}$	7/2	34.456	3.76×10^{-11}
35	$4s4p4d^o$	$4s\ 4p_{3/2}[1]4d_{3/2}$	5/2	34.528	3.92×10^{-11}
36	$4s4p4d^o$	$4s\ 4p_{3/2}[1]4d_{3/2}$	3/2	34.537	4.90×10^{-11}
37	$4s4p4d^o$	$4s\ 4p_{3/2}[1]4d_{5/2}$	5/2	34.631	4.52×10^{-11}
38	$4s4p4d^o$	$4s\ 4p_{3/2}[1]4d_{3/2}$	1/2	35.180	4.94×10^{-11}
39	$4s4p4d^o$	$4s\ 4p_{3/2}[1]4d_{5/2}$	3/2	35.252	4.99×10^{-11}

level which cannot decay through strong electric dipole ($E1$) transitions belongs to the $4s4p4d$ configuration. The decay of $4s4p_{3/2}\,(J=2)\,4d\ J=9/2$ level (index 16) to the lower levels of $4s4p^2$ or $4s^24d$ configurations by the $E1$ transitions is restricted by the $\triangle J=\pm 1$ selection rule. The theoretical lifetime of this level obtained in the single configuration approximation is 0.895 s. The magnetic quadrupole ($M2$) radiative transitions to the levels $4s\ 4p^2_{3/2}(2)J=5/2$ ($A^r=3.00\times10^{-1}$ s^{-1}, index 4) and $4s\ 4p_{1/2}(1)4p_{3/2}J=5/2$ ($A^r=4.16\times10^{-1}$ s^{-1}, index 6) are the strongest decay options for this level. The $M2$ radiative decay to the $4s^24d_{5/2}$ level is weaker by an order of magnitude ($A^r=2.29\times10^{-2}$ s^{-1}, index 11).

Our calculations show that electron-impact ionization cross sections for the long-lived $4s4p_{3/2}\,(J=2)\,4d_{3/2}J=9/2$ level are about three times higher than experimental values. As well, the cross sections start at about 17 eV, while experimental single-ionization threshold corresponds to 42.2 ± 1.8 [8]. This demonstrates that contribution from this level was not observed in the experiment. Additionally, we do not consider ionization from the first two excited configurations studied in [15] as their lifetimes are very small compared to the time ions need to reach the reaction zone with electron beam from the electron-cyclotron-resonance ion source [25].

Figure 1 shows configurations whose energy levels straddle the single-ionization threshold. All four configurations of the Se^{3+} ion correspond to excitations from the $4s$ shell. Only one of four configurations has subconfigurations with average energies above the ionization threshold. The configurations produced by excitations from the $3d$ shell are above the single-ionization threshold. In addition, the energy levels of

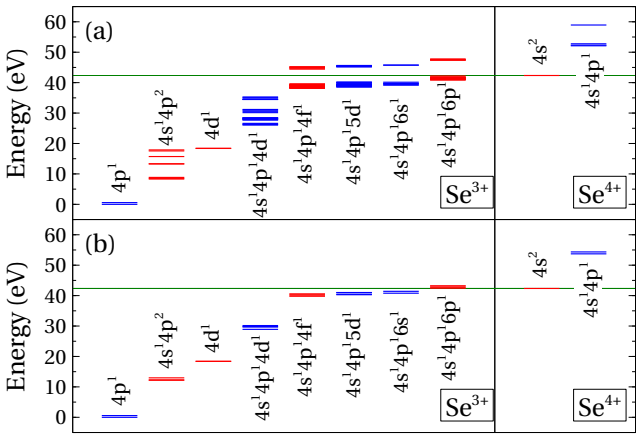

FIG. 1. Energy levels (a) and subconfigurations (b) of four lowest configurations and configurations that straddle the ionization threshold for the Se^{3+} ion. The ground and first excited configurations of Se^{4+} are also presented. Red (light)—even configurations; blue (dark)—odd configurations.

the ground and the first excited configurations for the Se^{3+} and Se^{4+} ions are presented in Fig. 1.

Our obtained electron-impact ionization cross sections for the ground level corresponding to the DI, EA, and REDA processes are compared with experimental values in Fig. 2. The DI cross sections are obtained in the potential of the ionized ion. Contribution of the radiative damping to the cross sections of the indirect process is negligible. The indirect process compared to the direct one dominates at the lower and intermediate energies of the incident electron. However, EA influence diminishes at the higher energies, especially when ionization from the $3d$ shell appears on the scene. It has to be noted that ionization from the $3d$ shell has the largest contribution to the total cross sections compared to the ionization from the valence $4s$ and $4p$ shells. Previous calculations for Se^{3+} have been performed using the CADW method [14]. Thus we also investigated the ionization process using the subconfiguration-averaged DW method and found

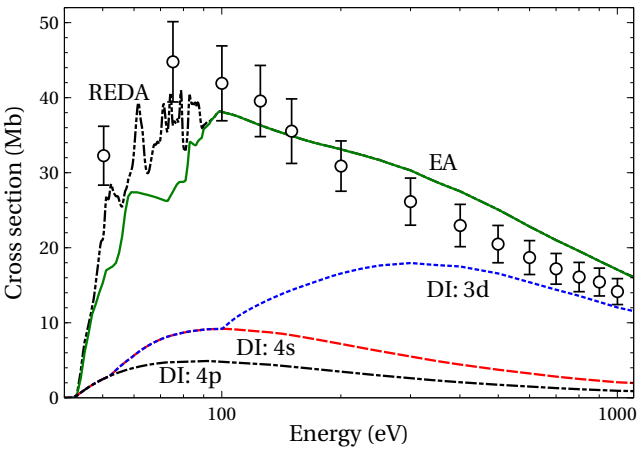

FIG. 2. Single ionization cross sections for the DI, EA, and REDA processes. Experiment: open circles with error bars [9]. Logarithmic scale is used for electron energies.

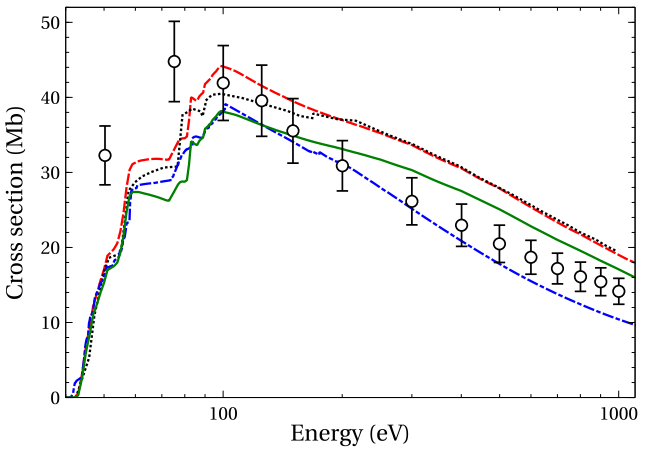

FIG. 3. Comparison of the total single-ionization cross sections (DI+EA). Our LLDW data are obtained in the potential of the ionized (green solid) and ionizing (red dashed) ions; dotted line (black) represents CADW values [14] and dashed-dotted line (blue) represents LLDW [15]. Experiment: open circles with error bars [9]. Logarithmic scale is used for electron energies.

good agreement among both our values for all energies of the incident electron.

Comparison of our LLDW results to the CADW [14] and previous LLDW [15] calculations for the ground level is given in Fig. 3. REDA data are not shown here as this effect has not been investigated before. Two our total cross sections are presented. In one case, DI is studied in the potential of ionized ion, while in another the potential of the ionizing ion is used.

CADW cross sections are mainly below our data obtained in the potential of ionizing ion at the lower and medium energies of the incident electron. Surprisingly, good agreement among the CADW and our cross sections is observed at the higher energies. It should be noted that the incident and scattered electrons are studied in the potential of the ionizing ion and the ejected electrons are calculated in the potential of the ionized ion for the CADW data [14]. This can be the reason for a difference among the DI values obtained from CADW [14] and our LLDW calculations. The CADW values are higher by about 40 % compared to our data calculated in the potential of the ionized ion. The difference of about 15% from the CADW calculations is obtained for the cross sections studied in the potential of the ionizing ion. The similar effect for the DI process has been observed in the study of the tungsten ions [17,18]. What is more, our EA data include excitations up to shells with $n = 25$, while the CADW values correspond to the excitations up to $n \leqslant 8$ [14]. Therefore, the lower contribution of EA to the total ionization cross sections is compensated by the higher influence of the DI process in the CADW calculations.

The difference among our LLDW values and LLDW results presented in [15] is seen in Fig. 3. At the higher energies of the incident electron this can be explained by the fact that ionization from the $3d$ shell is not included in the previous calculations. It was stated that produced configuration decays to Se^{5+}. However, the $3d^94p$ configuration is below the double-ionization threshold [14] and, thus, DI results in Se^{4+}.

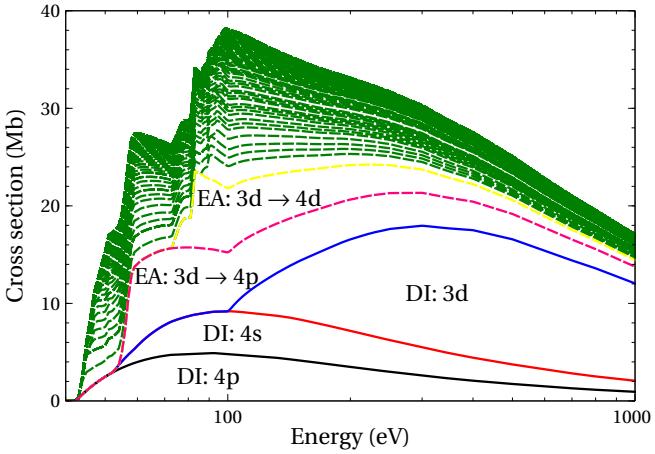

FIG. 4. Comparison of contribution from the DI and EA channels for single ionization of Se^{3+}. Logarithmic scale is used for electron energies.

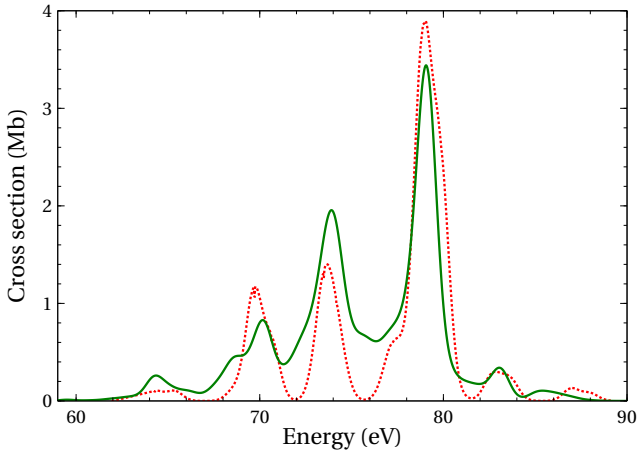

FIG. 5. REDA cross sections corresponding to DC to $3d^9 4s^2 4p\ 5l\ 5l'$ ($l, l' = 0$–4) configurations. Solid line (green) represents level-to-level calculations; dotted line (red) represents values for subconfigurations which are shifted by 1.6 eV to the higher-energy side for better agreement with the level-to-level data.

It should be noted that the main reason for the difference among these data is that the mean configuration in the previous calculations is generated by both the ground configurations of Se^{3+} and Se^{4+} to obtain potential of bound and continuum electrons. This leads to much higher DI cross sections in their calculations. For example, the DI $4s$ cross sections are higher by about 40% compared to our values calculated in the potential of ionized ion.

Figure 4 shows the main contributions of the EA channels compared to DI. The strongest EA channels correspond to $3d \rightarrow 4p$ and $3d \rightarrow 4d$ excitations. These two excitations make just slightly less than half of the total ionization cross sections for indirect process. The other EA channels separately provide much smaller contribution compared to the strongest ones. However, a large number of the weaker channels accounts for the significant part of the indirect process.

It has to be noted that the excitations from the $3p$ shell are opened at around 164 eV. However, excitations from the $3p$ shell are well above the double-ionization threshold and Auger cascade can lead to the higher ionization stages than Se^{4+}. For example, the Auger cascade from the $3p^5 4p^2$ configuration produced by the $3p \rightarrow 4p$ excitation leads to transfer of half of the initial population to the Se^{5+} ion. Thus the excitations to the higher shells would produce the larger yield of the Se^{5+} ion or even of the higher ionization stages. Furthermore, it was demonstrated that correlation effects have large importance in the study of the Auger cascades [26–28]. Only proper inclusion of correlation effects can provide good agreement with experiment for the ion yield. Based on this, we conclude that EA contribution from the $3p$ shell considered in the previous study [14] has to be omitted as it mainly leads to the higher ionization stages.

Large contribution of the REDA process at the lower energies of the incident electron is seen in Fig. 2. The REDA process is studied by considering transitions among the levels. However, as explained below, the transitions among subconfigurations are investigated for the higher shells.

Transitions among the levels are analyzed for the $3d^9 4s^2 4p\ 4l\ nl'$ (l = 1–3, l' = 1–3 for $n = 4$, and l' = 0–4 for n = 5–25) configurations. Subconfigurations are investigated for n = 26–50.

Figure 5 compares REDA cross sections produced from the decay of the $3d^9 4s^2 4p\ 5l\ 5l'$ ($l = 0, \ldots, 4$, $l' = 0, \ldots, 4$) configurations by considering transitions among levels and subconfigurations. The values obtained by the subconfigurations are shifted by 1.6 eV to the higher energy side for better agreement with peaks from the level-to-level calculations. Therefore, the same shift is used for all REDA cross sections obtained from DC capture to the $3d^9 4s^2 4p\ 5l\ nl'$ ($n = 6, \ldots, 50$) configurations. It can be seen from Fig. 5 that there is a slight difference in heights and widths for the peaks from the different calculations. This can be explained by the fact that we consider the transitions among average energies of the subconfigurations. Our modeling does not include width and asymmetry of the line shapes [29,30]. Furthermore, the average energy of the Auger transitions among the levels of two subconfigurations differs from the difference of the average energies of the initial and final subconfigurations. Previously, the Auger zones have been introduced to consider participation of various levels of the initial and final subconfigurations in the Auger transition [29].

In the same way, DC leading to formation of the $3d^9 4s^2 4p\ 6l\ 6l'$ and $3d^9 4s^2 4p\ 6l\ nl$ ($l,l' = 0$–4, n = 7–50) configurations is estimated. For the first group of the configurations, level-to-level study has been performed. However, transitions among subconfigurations are considered for the second group of the configurations. The first group of the configurations is used to find out shift of energy for the REDA cross sections obtained for the subconfigurations. The DC to the $3d^9 4s^2 4p\ nl\ n'l'$ configurations with $n,n' > 6$ has not been considered because of a very small contribution produced.

The study revealed that DC to the $4s\ 4p\ nl\ n'l'$ configurations with subsequent Auger cascade can lead to a single ionization of Se^{3+} starting from $nl = 6s$, $n'l' = 7f$, $nl = 6p$, $n'l' = 6f$, $nl = 6f$, $n'l' = 6f$, and $nl = 6g$, $n'l' = 6g$. Transitions among levels and subconfigurations are

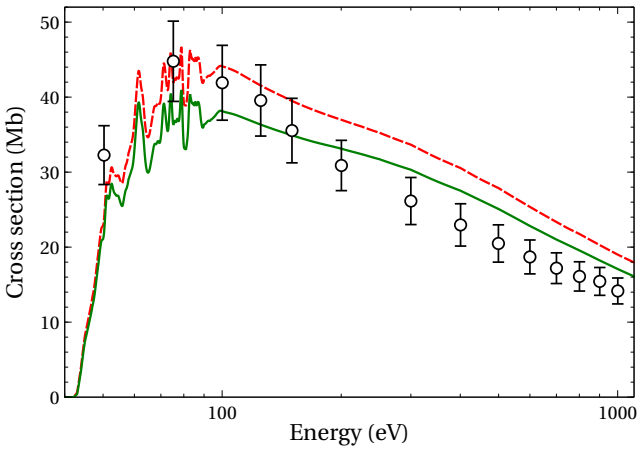

FIG. 6. Single-ionization cross sections obtained in the potential of ionized (green solid) and ionizing (red dashed) ion. Experiment: open circles with error bars [9]. Logarithmic scale is used for electron energies.

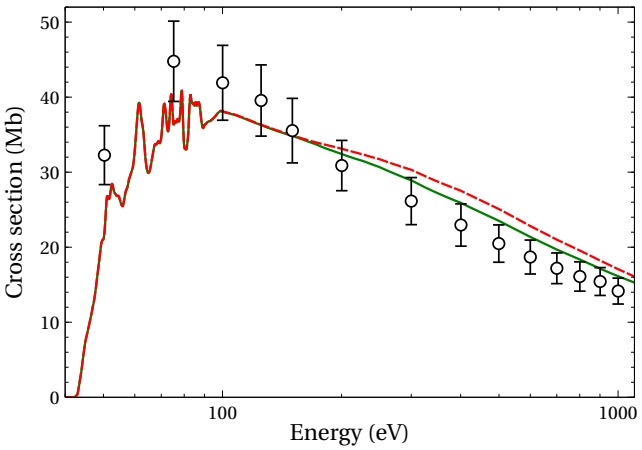

FIG. 7. Single-ionization cross sections obtained in the potential of ionized ion (red dashed) with subtracted experimental cross sections from double-ionization process (green solid). Experiment: open circles with error bars [9]. Logarithmic scale is used for electron energies.

investigated for $n = 7$–9 and $n \leqslant n' \leqslant 50$ in the same way as described above.

The current study omits the DC process which involves deeper shells than $3d$ since their contribution to a single-ionization cross section starts at the higher energies and is much smaller than the above-mentioned ones.

It can be seen from Fig. 2 that the theoretical cross sections are still below experimental error bars at the lower energies of the incident electron. Study which involves the DI cross sections obtained in the potential of the ionized ion demonstrates good agreement with experiment for this energy range (Fig. 6). Unfortunately, both calculations are above the experimental values at the high energy side. This can be explained by the fact that part of the produced Se^{4+} ions manage to reach a higher ionization stage, for example, due to knock off of an additional electron by the scattered or ejected electrons [6,7,31]. This process diminishes the obtained single-ionization cross sections. The current study does not include the direct double-ionization process when an additional electron is removed from the system due to additional ionization by the scattered or ejected electrons. To approximately estimate this situation, theoretical cross sections obtained in the potential of the ionized ion for the single-ionization process are subtracted by theoretical ones for the direct double-ionization process taken from [14] (Fig. 7). In this case, theoretical cross sections are slightly above the experimental error bars at the higher energies. The remaining difference among theoretical and experimental values can be explained by decay of the $3d^9 4s^2 4p$ configuration to the next ionization stage due to correlation effects. Previous studies for Auger cascades demonstrated importance of correlation effects producing higher ionization stages [26–28]. We have estimated transfer of population due to Auger decay of the $3d^9 4s^2 4p$ configuration to Se^{5+} using the configuration-interaction (CI) method. Admixed configurations are obtained using configuration-interaction strength [32–35]. This approach was also successfully used for the study of radiative transitions [33–35]. The current study with five admixed configurations ($4s7f$, $3d^9 4p^3$, $4p5d$, $3d^9 4s4p4d$, $3d^9 4s4p5d$) demonstrates, for example, that ionization cross sections diminish by about 0.3 Mb at an energy of 500 eV. This suggests that the larger CI basis could lead to the larger effect.

What is more, the theoretical values for direct double ionization were obtained for the case when one of the electrons takes all the excess energy after the first ionization process [14]. Our previous studies showed that better agreement with measurements at the higher energies is obtained for a situation when the ejected and scattered electrons share equally the excess energy [6]. However, cross sections of the direct double-ionization process in this case are higher by several times compared to the first scenario. Therefore, in this case, the lower single-ionization cross sections would be obtained.

It has to be noted that the theoretical data corresponding to the potential of the ionizing ion are within experimental error bars at the lower energies of the incident electron (Fig. 8). On the other hand, better agreement with experiment at the

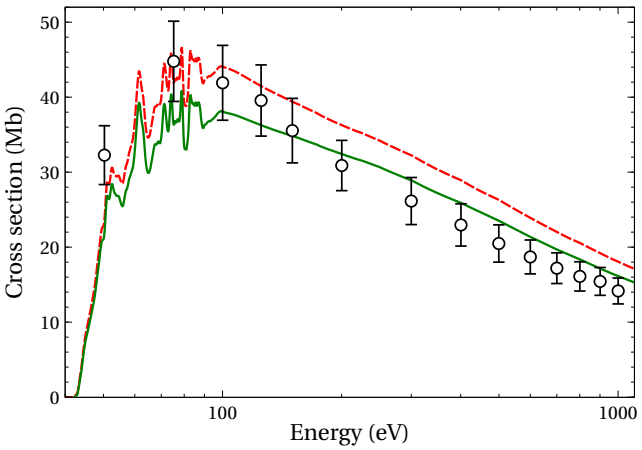

FIG. 8. Single-ionization cross sections obtained in the potential of ionized (green solid) and ionizing (red dashed) ion with subtracted experimental cross sections from double-ionization process. Experiment: open circles with error bars [9]. Logarithmic scale is used for electron energies.

higher energies is provided by calculations in the potential of the ionized ion. This agrees with the idea that both electrons are still in the vicinity of the ion at the lower energies of the incident electron. Thus the potential of the ionizing ion best fits to describe the ionization process. At the higher energies, the electrons are far away from the ion and continuum orbitals of the electrons have to be evaluated in the potential of the ionized ion.

IV. CONCLUSIONS

Single-ionization cross sections of the Se^{3+} ion have been studied using the DFS approximation. The study includes DI, EA, and REDA processes. Ionization from the $3d$, $4s$, and $4p$ shells determines the cross sections for the DI process. It is shown that excitations from the $3d$ shell to the $4p$ and $4d$ shells with subsequent autoionization are the strongest channels for the EA process. These excitations account for about 45% of the EA process at the peak value.

Large contribution from the REDA process is obtained at the lower energies of the incident electron. The theoretical cross sections are just above experimental error bars at the higher energies when the contribution to the ionization-ionization processes is subtracted. This suggests an idea that the double ionization of the Se^{2+} ion is mainly determined by the ionization-ionization and ionization-excitation-ionization processes.

The agreement with experiment at the lower energies of the incident electron is only obtained when the ionization process is investigated in the potential of the ionizing ion. On the other hand, study in the potential of the ionized ion provides good agreement with experiment for the higher energies of the electron.

ACKNOWLEDGMENTS

Part of the computations was performed on resources at the High Performance Computing Center HPC Saulėtekis in Vilnius University Faculty of Physics.

[1] N. C. Sterling and H. L. Dinerstein, Astrophys. J., Suppl. Ser. **174**, 158 (2008).
[2] A. L. Mashburn, N. C. Sterling, S. Madonna, H. L. Dinerstein, I. U. Roederer, and T. R. Geballe, Astrophys. J. **831**, L3 (2016).
[3] N. C. Sterling, S. Madonna, K. Butler, J. García-Rojas, A. L. Mashburn, C. Morisset, V. Luridiana, and I. U. Roederer, Astrophys. J. **840**, 80 (2017).
[4] M. S. Pindzola, F. Robicheaux, S. D. Loch, J. C. Berengut, T. Topcu, J. Colgan, M. Foster, D. C. Griffin, C. P. Ballance, D. R. Schultz *et al.*, J. Phys. B **40**, R39 (2007).
[5] J. Colgan and M. Pindzola, Eur. Phys. J. D **66**, 284 (2012).
[6] V. Jonauskas, A. Prancikevičius, Š. Masys, and A. Kynienė, Phys. Rev. A **89**, 052714 (2014).
[7] J. Koncevičiūtė and V. Jonauskas, Phys. Rev. A **93**, 022711 (2016).
[8] G. A. Alna'washi, K. K. Baral, N. B. Aryal, C. M. Thomas, and R. A. Phaneuf, J. Phys. B **47**, 105201 (2014).
[9] G. A. Alna'washi, N. B. Aryal, K. K. Baral, C. M. Thomas, and R. A. Phaneuf, J. Phys. B **47**, 135203 (2014).
[10] D. A. Esteves, R. C. Bilodeau, N. C. Sterling, R. A. Phaneuf, A. L. D. Kilcoyne, E. C. Red, and A. Aguilar, Phys. Rev. A **84**, 013406 (2011).
[11] N. C. Sterling, D. A. Esteves, R. C. Bilodeau, A. L. D. Kilcoyne, E. C. Red, R. A. Phaneuf, and A. Aguilar, J. Phys. B **44**, 025701 (2011).
[12] D. A. Esteves, A. Aguilar, R. C. Bilodeau, R. A. Phaneuf, A. L. D. Kilcoyne, E. C. Red, and N. C. Sterling, J. Phys. B **45**, 115201 (2012).
[13] D. A. Macaluso, A. Aguilar, A. L. D. Kilcoyne, E. C. Red, R. C. Bilodeau, R. A. Phaneuf, N. C. Sterling, and B. M. McLaughlin, Phys. Rev. A **92**, 063424 (2015).
[14] M. S. Pindzola and S. D. Loch, J. Phys. B **49**, 125202 (2016).
[15] L. Liu, P. Liu, and J. Zeng, J. Electron Spectrosc. Relat. Phenom. **209**, 9 (2016).
[16] D.-H. Zhang and D.-H. Kwon, J. Phys. B **47**, 075202 (2014).
[17] V. Jonauskas, A. Kynienė, G. Merkelis, G. Gaigalas, R. Kisielius, S. Kučas, Š. Masys, L. Radžiūtė, and P. Rynkun, Phys. Rev. A **91**, 012715 (2015).
[18] A. Kynienė, Š. Masys, and V. Jonauskas, Phys. Rev. A **91**, 062707 (2015).
[19] M. F. Gu, Can. J. Phys. **86**, 675 (2008).
[20] R. D. Cowan, *The Theory of Atomic Structure and Spectra* (University of California Press, Berkeley, CA, 1981).
[21] A. Müller, in *Advances In Atomic, Molecular, and Optical Physics*, edited by P. R. B. Ennio Arimondo and C. C. Lin (Academic Press, New York, 2008), Vol. 55, pp. 293–417.
[22] A. Kramida, Yu. Ralchenko, J. Reader, and NIST ASD Team, NIST atomic spectra database (version 5.4), 2016.
[23] A. Müller, Atoms **3**, 120 (2015).
[24] A. Borovik, Jr., M. F. Gharaibeh, S. Schippers, and A. Müller, J. Phys. B **48**, 035203 (2015).
[25] A. Borovik, C. Brandau, J. Jacobi, S. Schippers, and A. Müller, J. Phys. B **44**, 205205 (2011).
[26] V. Jonauskas, R. Karazija, and S. Kučas, J. Phys. B **41**, 215005 (2008).
[27] J. Palaudoux, P. Lablanquie, L. Andric, K. Ito, E. Shigemasa, J. H. D. Eland, V. Jonauskas, S. Kučas, R. Karazija, and F. Penent, Phys. Rev. A **82**, 043419 (2010).
[28] V. Jonauskas, S. Kučas, and R. Karazija, Phys. Rev. A **84**, 053415 (2011).
[29] S. Kučas, R. Karazija, V. Jonauskas, and S. Aksela, Phys. Scr. **52**, 639 (1995).
[30] V. Jonauskas, L. Partanen, S. Kučas, R. Karazija, M. Huttula, S. Aksela, and H. Aksela, J. Phys. B **36**, 4403 (2003).
[31] M. Gryziński, Phys. Rev. **138**, A336 (1965).
[32] R. Karazija and S. Kučas, J. Quant. Spectrosc. Radiat. Transfer **129**, 131 (2013).
[33] A. Kynienė, V. Jonauskas, S. Kučas, and R. Karazija, Lith. J. Phys. **48**, 219 (2008).
[34] V. Jonauskas, R. Kisielius, A. Kynienė, S. Kučas, and P. H. Norrington, Phys. Rev. A **81**, 012506 (2010).
[35] V. Jonauskas, G. Gaigalas, and S. Kučas, At. Data Nucl. Data Tables **98**, 19 (2012).